HHS Public Access

Author manuscript

*JACC Cardiovasc Interv*. Author manuscript; available in PMC 2017 September 26.

Published in final edited form as:

*JACC Cardiovasc Interv*. 2016 September 26; 9(18): 1953–1965. doi:10.1016/j.jcin.2016.06.054.

# Elimination of Trans-coarctation Pressure Gradients Has No Impact on Left Ventricular Function or Aortic Shear Stress Post Intervention in Patients with Mild Coarctation

**Zahra Keshavarz-Motamed, PHD**[1], **Farhad Rikhtegar Nezami, PHD**[1], **Ramon A. Partida, MD**[1,2], **Kenta Nakamura, MD**[1,2], **Pedro Vinícius Staziaki, MD**[2], **Eyal Ben-Assa, MD**[1], **Brian Ghoshhajra, MD**[2], **Ami B. Bhatt, MD, FACC**[2], and **Elazer R. Edelman, MD, PHD, FACC, FAHA**[1,3]

[1]Institute for Medical Engineering and Science, Massachusetts Institute of Technology, Cambridge, MA, USA

[2]Cardiovascular Division, Massachusetts General Hospital, Harvard Medical School, Boston, MA, USA

[3]Cardiovascular Division, Brigham and Women's Hospital, Harvard Medical School, Boston, MA, USA

## Abstract

**OBJECTIVES—**To investigate the impact of transcatheter intervention on left ventricular (LV) function and aortic hemodynamics in patients with mild coarctation of the aorta (COA).

**BACKGROUND—**The optimal method and timing of transcatheter intervention for COA remains unclear, especially when the severity of COA is mild (peak-to-peak trans-coarctation pressure gradient, $P_K dP < 20$ mmHg). Debate rages regarding the risk/benefit ratio of intervention *vs.* long-term effects of persistent minimal gradient in this heterogeneous population with differing blood pressures, ventricular function and peripheral perfusion.

**METHODS—**We developed a unique computational fluid dynamics and lumped parameter modeling framework based on patient-specific hemodynamic input parameters and validated it against patient-specific clinical outcomes (pre- and post-intervention). We used clinically measured hemodynamic metrics and imaging of the aorta and the LV in thirty-four patients with mild COA to make these correlations.

**RESULTS—**Despite dramatic reduction in trans-coarctation pressure gradient (catheter and Doppler echocardiography pressure gradients reduced 75% and 47.3%,), there was only modest effect on aortic flow and no significant impact on aortic shear stress (maximum time-averaged wall shear stress in descending aorta was reduced 5.1%). In no patient did transcatheter intervention improve LV function (e.g., stroke work and normalized stroke work were reduced by only 4.48% and 3.9%).

Addresses for correspondence: Dr. Zahra KESHAVARZ MOTAMED; Institute for Medical Engineering and Science, Massachusetts Institute of Technology, Cambridge, MA, USA. Address: 77 Massachusetts Avenue, Building E25-438, Cambridge, MA 02139, USA. zahra_km@MIT.EDU; Telephone: (+1) 617-981-2642.

**Conflict of interest**: There are no conflicts of interest. There are no relationships with industry.

**CONCLUSIONS—**Transcatheter intervention which successfully relieves mild COA pressure gradients does not translate to decrease myocardial strain. The effects of intervention were determined to the greatest degree by ventricular-vascular coupling hemodynamics, and provide a novel valuable mechanism to evaluate patients with COA which may influence clinical practice.

### Keywords

Mild coarctation; Peak to peak pressure gradient; Transcatheter intervention; Left ventricle function; Aortic hemodynamics

## INTRODUCTION

Coarctation of the aorta (COA) is a narrowing of the descending aorta which classically occurs near the takeoff of the left subclavian artery. There are many morphologic variants and the most diffuse forms may involve the aortic arch or isthmus to varying degrees. Individuals with coarctation demonstrate a diffuse arteriopathy with elastic fiber fragmentation, increased collagen deposition in the coarctation segment and ascending aorta as well as abnormalities of arterial compliance and endothelial function (1,2,3,4). The hemodynamic severity and clinical manifestations of COA vary from asymptomatic mild narrowing of the aortic isthmus to severe obstruction with left ventricular failure (1,2,3,4). Symptoms emerge with severity - 60% of adults over 40 years with uncorrected COA develop heart failure, 75% die by the age of 50, and 90% by the age of 60 (5).

A hemodynamically significant COA is often defined as a catheter peak-to-peak pressure gradient or resting or exercise Doppler pressure gradient of 20 mmHg across the site of coarctation. Importantly, individuals with repaired coarctation without significant anatomic evidence for narrowing may demonstrate a gradient with exertion secondary to a lack of compliance at the anastomotic site as flow to the descending aorta increases with leg exercises (6,7).

While COA is readily diagnosed and interventional and surgical therapies implemented, areas of contention and uncertainty remain. The optimal method and timing of the intervention remain undefined especially when the severity of COA is mild (peak-to-peak trans-coarctation pressure gradient, $P_K dP < 20$ mmHg) (8), given the balance of risks for early and late mortality and reoperation (9,10). While most cardiologists agree that a $P_K dP$ greater than 20 mmHg warns of severe COA and warrants interventional/surgical repair, it is unclear whether a mild degree of COA can be accepted or portends long term arterial compliance, endothelial function, hypertension or renal perfusion issues (8,11,12,13). Some groups suggest that treatment strategies for patients with mild COA may need to be redefined as transcatheter interventions emerge (14). Most patients with mild COA are suitable candidates for transcatheter treatment, which can be performed with very low morbidity, resulting in an almost complete elimination of the pressure gradient in 95% of the patients (15,16). Yet, there is also the emerging observation that relief of the pressure gradient does not correlate with relief of symptoms or functional improvement. An understanding of the clinical and physiologic effects of relieving aortic gradients in mild COA is needed before changing current treatment recommendations (8,12).

The aim of this study was to investigate the impact of transcatheter intervention in patients with mild COA. We developed a unique computational fluid dynamics and lumped parameter modeling framework based on patient-specific hemodynamic input parameters and validated with patient-specific clinical outcomes that predicted left ventricle (LV) function and aortic hemodynamics of patients with mild COA (pre- and post-intervention). We used clinically measured hemodynamic metrics and imaging of the aorta and the left ventricle (LV) (Doppler echocardiography, cardiac catheterization, computed tomography (CT) and magnetic resonance (MR) imaging) in thirty-four patients with mild COA to make these correlations.

## METHODS

### STUDY POPULATION

This was a retrospective clinical study of individuals with COA who underwent transcatheter intervention at a single institution (Massachusetts General Hospital, Boston, MA, USA). Measurements were performed according to the American College of Cardiology & American Heart Association guidelines. The protocol was reviewed and approved by the Ethics Committee of Massachusetts General Hospital, Boston, MA, USA. All patients provided written informed consent under the supervision of the Institutional Review Board.

Thirty-four adult patients with mild COA, ages 22 to 61 years (mean: 41 ± 10.5) referred to Massachusetts General Hospital between 2006 and 2014, were included in this study. Measured patients characteristics (Table 1) included: mean systolic blood pressure (139 ± 22.5 mmHg), diastolic blood pressure (79 ± 11.7 mmHg), COA diameter (13.2 ± 4.5 mm) and diameter ratio (COA/Aorta) (0.72 ± 0.25). Associated cardiovascular lesions included bicuspid aortic valve (ten patients), mild and moderate tricuspid aortic valve stenosis (three patients), unicuspid valve (one patient), ventricular septal defect (one patient), mitral valve regurgitation (four patients), descending aorta aneurysms (six patients) and collateral circulation (two patients).

### INTERVENTIONAL CARDIAC CATHETERIZATION

Cardiac catheterization was performed to determine the exact morphology and the pressure gradient of the COA in all patients. Angiography was performed in lateral and anteroposterior or left anterior oblique projections. Measurements of the aorta were made and averaged at five different sites: ascending aorta, isthmus proximal coarctation, coarcted region, descending aorta distal to the coarctation as well as at the level of the diaphragm. For the assessment of COA, the pullback systolic pressure gradients including peak to peak pressure gradients obtained across the COA site and angiography were used to choose appropriate stents. Exclusion criteria were 1) long tubular coarctation segment which were referred for surgical repair; 2) any patient underwent additional procedure (e.g., surgical correction and balloon angioplasty); 3) pseudocoarctation.

All patient population included in this study (34 described above) underwent percutaneous aortic stent placement (20 direct stenting, 14 pre-dilated with a balloon). Stent types used included IntraStent LD Family, Atrium and Cordis Palmaz Genesis. The geometrical

information (diameter & length) of the stents and balloons were (diameter: 12.8 ± 3.3 mm & length: 32.8 ± 5.11 mm) and (diameter: 17.4 ± 6.8 mm & length: 34.6 ± 8.4 mm), respectively (Table 1). There was no evidence of aortic atherosclerotic disease, aortic dissection, intramural hematoma or anomalous coronary arteries. Furthermore, there was no evidence of any fluid collection within the mediastinum, the pericardium or the pleura. In all patients, except patient No. 1, the final angiogram revealed a well deployed stent without residual stenosis. All patients tolerated the procedure well with no complications to report.

## TRANSTHORACIC DOPPLER-ECHOCARDIOGRAPHY (TTE)

TTE exams were performed and analyzed by experienced echocardiographers with a commercially available echocardiography machine (Philips iE33 ultrasound system, Koninklijke Philips, Amsterdam, Netherlands), and conducted according to the American Society of Echocardiography guidelines. Metrics included:

a. **Valve hemodynamic parameters:** transvalvular pressure gradients were determined by the Bernoulli formula. The left ventricle outflow track (*LVOT*) diameter, *LVOT* flow velocity measured by pulsed-wave Doppler, the aortic transvalvular jet velocity measured by continuous-wave Doppler and valve effective orifice area (EOA) using the continuity equation as follows,

$$EOA_{TTE} = \frac{SV_{LVOT}}{VTI_{AO}} = \frac{(VTI_{LVOT} \times A_{LVOT})}{VTI_{AO}} \quad (1)$$

where $SV_{LVOT}$, $A_{LVOT}$ and $VTI_{LVOT}$ are the stroke volume measured in the LVOT, the cross-sectional area of the LVOT, and the velocity-time integral of the LVOT, respectively.

b. **Vascular hemodynamic parameters**: the systemic arterial compliance (SAC) and the systemic vascular resistance (SVR) (7,17);

$$SAC = SV_i / PP \quad (6)$$

$$SVR = 80 MAP / CO \quad (7)$$

where $SV_i$, PP, MAP, and CO are stroke volume indexed by the body surface area, pulse pressure, mean arterial pressure and cardiac output, respectively.

c. **COA hemodynamic parameters**: Trans-coarctation pressure gradients were determined by the Bernoulli formula. Measurements of the aorta were made and averaged at five different sites: ascending aorta, isthmus proximal coarctation, coarcted region, descending aorta distal to the coarctation as well as at the level of the diaphragm.

### STATISTICAL ANALYSIS

Results were expressed as mean ± standard deviations (SD). Statistical analyses were performed using SigmaStat software (Version 3.1, Systat Software, SanJose, CA, USA). Paired student's t-test was used to detect any significant hemodynamic difference between pre-intervention and post-intervention conditions in patients with mild COA.

### NUMERICAL STUDY

We developed a special computational fluid dynamics model using large eddy simulation (LES) and lumped parameter modeling framework (Figures 1 and 2). LV function and aortic fluid dynamics were predicted in all thirty-four patients with mild COA (pre- and post-intervention) using patient-specific boundary conditions. Numerical calculations were validated against clinical cardiac catheterization and Doppler echocardiography data in all thirty-four patients with mild COA (see Figures 4 to 7 for examples). Please refer to the Appendix for all details related to the numerical study.

## RESULTS

### CLINICAL ASSESSMENT OF HEMODYNAMICS: DOPPLER ECHOCARDIOGRAPHY AND CATHETER PRESSURE GRADIENTS

Both Doppler and direct catheter measures documented a trans-coarctation pressure gradient in all patients with mild COA (Table 1, Figure 3) which were significantly reduced by transcatheter intervention. Catheter peak to peak pressure gradient and Doppler echocardiography pressure gradient were reduced by 75% and 47.3%, respectively (N=34; $p < 0.05$). Numerical simulation of the peak velocity downstream of the COA correlated well with Doppler echocardiographic measurements in all thirty-four patients with a maximum relative error of 5.2% (Figures 5 and 7). There was a good agreement between the pressure waveforms upstream and downstream of the COA obtained from simulations and catheter data in all thirty-four patients with a maximum relative error of peak-to-peak pressure gradient of 3.8% (Figures 4 and 6).

### HEMODYNAMICS: AORTIC FLUID DYNAMICS AND LEFT VENTRICULAR FUNCTION

Mild COA alters the flow dynamics in the aorta (Figures 5 and 7) which contributes to elevated wall shear stress mostly distal to the COA. Shear stress exerted on the aorta wall was determined to be reduced modestly by intervention. Computed mean and maximum time-averaged wall shear stress (TAWSS) in descending aorta were reduced by 19.4% and 5.1%, respectively (N=34; $p < 0.05$) (Figures 5, 7 and 8). Similarly mean and maximum oscillatory shear index (OSI) in the descending aorta were reduced by 13.3% and 10.1%, respectively; N=34; $p < 0.05$ (Figures 5, 7 and 9) moving the flow slightly farther from pure oscillatory to more stable domains.

These modest effects on the aortic flow were not accompanied by significant reduction in LV function parameters as ventricular pressure, stroke work, and normalized stroke work (the energy required to eject 1 mL of blood through the valvulo-arterial system) were statistically but not dramatically different pre and post intervention conditions (Figures 4, 6

and 10). Stroke work, normalized stroke work and peak LV pressure were reduced by only 4.48%, 3.9% and 3.8% (N=34, $p < 0.05$), respectively.

## DISCUSSION

We sought to determine if the relief of mild trans-coarctation pressure gradient resulted in a significant physiologic improvement in metrics of aortic hemodynamics and left ventricular function in patients with mild COA, and found no such benefit. Despite a dramatic reduction in the pressure gradient, there was at best a modest effect improvement on the aortic flow and no real impact on aortic shear stress in all thirty-four patients with mild COA. In none of the thirty-four patients with mild COA who did transcatheter intervention LV hemodynamic condition or function was improved. In current clinical practice, the decision to intervene in low gradient coarctation cases is often based on factors such as arm-leg blood pressure gradients (18), exercise induced drop in ankle brachial index, persistent or resistant systemic hypertension, presence of collateral arterial vessels, diastolic or systolic left ventricular dysfunction or symptoms of claudication, (19) but rarely discerned changes in physiological signals.

This is the first mechanistic insight into why abolishing the aortic gradient does not translate directly into improved aortic or left ventricular hemodynamics in these individuals. There are several specific findings which should be considered individually:

1. **Transcatheter intervention does not improve left ventricular function.** LV stroke work represents the energy that the ventricle delivers to the blood during ejection, and energy necessary to overcome the viscoelastic properties of the myocardium itself, and is an effective metric of LV load and clinical state. Our results reveal that though pre-intervention COA increases the burden on the left ventricle with augmented flow resistance, post-intervention the LV load does not improve as introducing a stent reduces the arterial systemic compliance, in fact increasing LV load. Intervention for mild COA therefore has limited utility in reducing myocardial strain. Previous studies have demonstrated persistent increased left ventricular mass and hypertrophy in long-term post COA intervention follow-up (20,21,22). Our results provide a potential mechanism for this common clinical dilemma.

2. **Transcatheter intervention improves modestly local aortic hemodynamics.** Our analysis of aortic flow patterns indicates that a mild COA increases shear stress and disturbs aortic flow, negatively affecting aortic hemodynamics. However, post-intervention, local hemodynamics were only moderately improved with persistently elevated shear stresses and non-uniformly distributed aortic flow disturbance. These hemodynamics have been demonstrated to worsen endothelial dysfunction, dedifferentiation of the arterial smooth muscle and medial thickening (23), while local aortic flow changes may lead to aortic wall abnormalities predisposing to complications such as aortic aneurysm (24,25,26,27) rupture (28,29) and dissection.

3. **Patients with mild COA have higher incidence of hypertension even after successful transcatheter interventions:** Patients with COA usually have upper extremity hypertension and are characterized by reduced systemic arterial compliance (30,31,32,33). We demonstrate that the systemic arterial compliance was further reduced (by 18.5% post intervention; N=34; $p < 0.05$; Figure 11) in patients with mild COA. This could partly explain why patients with COA may have hemodynamic abnormalities, such as systemic hypertension (34), abnormal exercise response (34,35), and hyperdynamic systolic function (36,37) even after successful COA intervention.

4. **Transcatheter intervention can effectively reduce $P_K$dP but $P_K$dP fails to reflect the effect of COA intervention on the LV and the aorta hemodynamics.** In current AHA guidelines, a $P_K$dP > 20 mmHg is an indication for interventional/surgical repair (32,33). Our results show that stent implantation can effectively reduce catheterization pressure gradient ($P_K$dP) as well as echocardiography pressure gradient. However, pressure gradients should be used with caution in patients with COA as we demonstrate that: 1) $P_K$dP fails to reflect the effects of the COA (pre intervention) and transcatheter intervention on the LV and aorta hemodyanmics; 2) catheter and echocardiography pressure gradients are highly influenced by the flow rate. They are reduced when the flow rate is decreased (7,38); 3) $P_K$dP is significantly influenced by arterial compliance. $P_K$dP increases with reduced proximal COA compliance but decreases with reduced systemic compliance (7).

## LIMITATIONS

The effect of coartation repair is largely understood through changes in the vascular bed and heart upstream of the lesion. Our study attempts to refine the current body of knowledge by highlighting the importance of left ventricular function and aortic hemodynamics rather than isolated, lesion-specific parameters such as pressure gradient in predicting benefit of coartation repair. Moreover, downstream effects, specifically renal and neurohormonal changes, are well-established in native coarctation (39,40,41,42) but poorly characterized following coarctation repair (43). Future studies must not only consider the upstream but also downstream effects of coartation repair when determining indication and assessing benefit of intervention. In addition, there is no available data for the antihypertensive management in our patients.

## CONCLUSIONS

The data presented in this study are based on a population of thirty-four patients with mild COA. Transcatheter intervention can effectively reduce the trans-coarctation pressure gradient however this results in only a modest local improvement in aortic hemodynamics, and does not translate at all to a concomitant improvement in LV hemodynamics or reduction in myocardial strain in all thirty-four patients with mild COA. The findings of this study suggest that beyond standard indices of evaluation of the severity of COA (e.g., catheter and echo pressure gradients), aortic local hemodynamic and LV function should be

considered to better identify the actual disease severity that may be masked by the post-intervention low pressure gradient phenomenon, specifically in a subset of patients with mild COA conditions. Whether these physiologic studies will provide insight into the mechanism of repair for more significant COA with higher gradients has yet to be evaluated. Moreover, our findings suggest that how the definition of “mild coarctation”, based on peak-to-peak trans-coarctation pressure gradient of 20 mmHg, is an oversimplification. This suggests that more accurate assessments of this class of patients are required for deciding about performing a transcatheter intervention.

## Supplementary Material

Refer to Web version on PubMed Central for supplementary material.

## Acknowledgments

ERE was supported in part by grants from the NIH (R01 GM 49039). ZKM is supported in part by American Heart Association postdoctoral fellowship (16POST26420039). Mohamed Youniss was responsible for data collection.

## ABBREVIATIONS LIST

| | |
|---|---|
| **COA** | Coarctation of the aorta |
| **$P_K dP$** | Peak-to-peak trans-coarctation pressure gradient |
| **LV** | Left ventricle |
| **SAC** | Systemic arterial compliance |
| **TAWSS** | Time-averaged wall shear stress |
| **OSI** | Oscillatory shear index |

## References

1. Abbott ME. Coarctation of the aorta of the adult type, II: a statistical and historical retrospect of 200 recorded cases with autopsy, of stenosis or obliteration of the descending arch in subjects above the age of two years. Am Heart J. 1928; 3:574–628.
2. Reifenstein GH, Levine SA, Gross RE. Coarctation of the aorta: a review of 104 autopsied cases of the “adult type,” 2 years of age or older. Am Heart J. 1947; 33:146–168. [PubMed: 20283558]
3. Vukovic I, Lackovic V, Todorivic V, Kanjuh V, Ilic S. Cytohistologic and immuno-histochemical characteristics of the aortic intima and media in coarctation of the aorta of the adult type. Srp Arh Celak Lek. 2004; 132(suppl 1):66–71.
4. Bhatt AB, Yeah DD. Long-term outcomes in coarctation of the aorta: an evolving story of success and new challenges. Heart. 2015; doi: 10.1136/heartjnl-2015-307641
5. Brickner ME, Hillis LD, Lange RA. Congenital heart disease in adults. NEJM. 2000; 342:256–263. [PubMed: 10648769]
6. Gunthard J, Buser PT, Miettunen R, Hagman A, Wyler F. Effects of morphologic restenosis, defined by MRI after coarctation repair, on blood pressure and arm-leg Doppler gradients. Angiology. 1996; 47:1073–1080. [PubMed: 8921756]
7. Keshavarz-Motamed Z, Edelman ER, Motamed PK, Garcia J, Dahdah N, Kadem L. The role of aortic compliance in determination of coarctation severity: lumped parameter modeling, *in vitro* study and clinical evaluation. J Biomech. 2015; 48:4229–4237. [PubMed: 26596718]

8. Marshall AC, Perry SB, Keane JF, Lock JE. Early results and medium-term follow-up of stent implantation for mild residual or recurrent aortic coarctation. Am Heart J. 2000; 139(6):1054–60. [PubMed: 10827387]
9. Oliver JM, Gallego P, Gonzalez A, Aroca A, Bret M, Mesa JM. Risk Factors for Aortic Complications in Adults With Coarctation of the Aorta. J Am Coll Cardiol. 2004; 44(8):1641–7. [PubMed: 15489097]
10. Brown ML, Burkhart HM, Connolly HM, Dearani JA, Cetta F, Li Z, Oliver WC, Warnes CA, Schaff HV. Coarctation of the Aorta: lifelong Surveillance Is Mandatory Following Surgical Repair. J Am Coll Cardiol. 2013; 62(11):1020–1025. [PubMed: 23850909]
11. Bouchart F, Dubar A, Tabley A, et al. Coarctation of the aorta in adults: surgical results and long-term follow-up. Ann Thorac Surg. 2000; 70:1483–8. [PubMed: 11093474]
12. Vriend JW, Zwinderman AH, de Groot E, Kastelein JJ, Bouma BJ, Mulder BJ. Predictive value of mild, residual descending aortic narrowing for blood pressure and vascular damage in patients after repair of aortic coarctation. Eur Heart J. 2005; 26(1):84–90. [PubMed: 15615804]
13. Rosenthal E. Coarctation of the aorta from fetus to adult: curable condition or life long disease process? Heart. 2005; 91:1495–1502. [PubMed: 16230458]
14. Rosenthal E. Stent implantation for aortic coarctation: the treatment of choice in adults? J Am Coll Cardiol. 2001; 38:1524–1527. [PubMed: 11691534]
15. Mullen MJ. Coarctation of the aorta in adults: do we need surgeons? Heart. 2003; 89:3–5. [PubMed: 12482776]
16. Zabal C, Attie F, Rosas M, et al. The adult patient with native coarctation of the aorta: balloon angioplasty or primary stenting? Heart. 2003; 89:77–83. [PubMed: 12482798]
17. Keshavarz-Motamed Z, Garcia J, Gaillard E, Capoulade R, LeVen F, Cloutier G, Kadem L, Pibarot P. Non-invasive determination of left ventricular workload in patients with aortic stenosis using magnetic resonance imaging and Doppler echocardiography. PLoS One. 2014; 9:e86793. [PubMed: 24489786]
18. Yetman AT, Nykanen D, McCrindle BW, et al. Balloon angioplasty of recurrent coarctation: a 12-year review. J Am Coll Cardiol. 1997; 30:811–816. [PubMed: 9283545]
19. Beekman RH, Rocchini AP, Behrendt DM, et al. Reoperation for coarctation of the aorta. Am J Cardiol. 1981; 48:1108–1114. [PubMed: 6975561]
20. Moskowitz WB, Schieken RM, Mosteller M, et al. Altered systolic and diastolic function in children after “successful” repair of coarctation of the aorta. Am Heart J. 1990; 120:103–109. [PubMed: 2360493]
21. Krogmann ON, Kramer HH, Rammos S, et al. Non-invasive evaluation of left ventricular systolic function late after coarctation repair: influence of early vs late surgery. Eur Heart J. 1993; 14:764–769. [PubMed: 8325302]
22. Johnson MC, Gutierrez FR, Sekarski DR, et al. Comparison of ventricular mass and function in early versus late repair of coarctation of the aorta. Am J Cardiol. 1994; 73:698–701. [PubMed: 8166068]
23. Menon A, Eddinger TJ, Wang H, Wendell DC, Toth JM, LaDisa JF. Altered hemodynamics endothelial function, and protein expression occur with aortic coarctation and persist after repair. Am J Physiol Heart Circ Physiol. 2012; 303:1304–1318.
24. Kirsh MM, Perry B, Spooner E. Management of pseudoaneurysm following patch grafting for coarctation of the aorta. J Thorac Cardiovasc Surg. 1977; 74:636–639. [PubMed: 578564]
25. Fung, YC. Mechanical properties of living tissues. Vol. 198. Springer; New York: p. 468
26. Parikh SR, Hurwitz RA, Hubbard JE, Brown JW, King H, et al. Preoperative and postoperative ‘aneurysm’ associated with coarctation of the aorta. J Am Coll Cardiol. 1991; 17:1367–1372. [PubMed: 2016456]
27. Liu S, Tang D, Tieche C, Alkema P. Pattern formation of vascular smooth muscle cells subject to nonuniform fluid shear stress: mediation by gradient cell density. Am J Physiol Heart Circ Physiol. 2003; 285:1072–1080.
28. Unger EL, Marsan RE. Ruptured aneurysm 20 years after surgery for coarctation of the aorta. Am J Roentgenol. 1977; 129:329–330. [PubMed: 409172]

29. Parks WJ, Ngo TD, Plauth WH Jr, Bank ER, Shepparda SK, et al. Incidence of aneurysm formation after Dacron patch aortoplasty repair for coarctation of the aorta: long-term results and assessment utilizing magnetic resonance angiography with three-dimensional surface rendering. J Am Coll Cardiol. 1995; 26:266–271. [PubMed: 7797761]
30. Gardiner HM, Celermajer DS, Sorensen KE, Georgakopoulos D, Robinson J, Thomas O, Deanfield JE. Arterial reactivity is significantly impaired in normotensive young adults after successful repair of aortic coarctation in childhood. Circulation. 1994; 89:1745–1750. [PubMed: 8149540]
31. Xu J, Shiota T, Omoto R, et al. Intravascular ultrasound assessment of regional aortic wall stiffness, distensibility, and compliance in patients with coarctation of the aorta. AM Heart J. 1997; 134:93–98. [PubMed: 9266788]
32. Brili S, Dernellis J, Aggeli C, Pitsavos C, Hatzos C, Stefanadis C, Toutouzas P. Aortic elastic properties in patients with repaired coarctation of aorta. Am J Cardiol. 1998; 82:1140–1143. [PubMed: 9817501]
33. Vogt M, Kühn A, Baumgartner D, Baumgartner C, Busch R, Kostolny M, Hess J. Impaired elastic properties of the ascending aorta in newborns before and early after successful coarctation repair: proof of a systemic vascular disease of the prestenotic arteries. Circulation. 2005; 111:3269–3273. [PubMed: 15956120]
34. Leandro J, Smallhorn JF, Benson L, et al. Ambulatory blood pressure monitoring and left ventricular mass and function after successful surgical repair of coarctation of the aorta. J Am Coll Cardiol. 1992; 20:197–204. [PubMed: 1607525]
35. Markel H, Rocchini AP, Beekman RH, et al. Exercise-induced hypertension after repair of coarctation of the aorta: arm versus leg exercise. J Am Coll Cardiol. 1986; 8:165–171. [PubMed: 3711512]
36. Kimball TR, Reynolds JM, Mays WA, et al. Persistent hyperdynamic cardiovascular state at rest and during exercise in children after successful repair of coarctation of the aorta. J Am Coll Cardiol. 1998; 24:194–200.
37. Carpenter MA, Dammann JF, Watson DD, et al. Left ventricular hyperkinesias at rest and during exercise in normotensive patients 2 to 27 years after coarctation repair. J Am Coll Cardiol. 1998; 6:879–886.
38. Keshavarz-Motamed Z, Garcia J, Maftoon N, Bedard E, Chetaille P, Kadem L. A new approach for the evaluation of the severity of coarctation of the aorta using Doppler velocity index and effective orifice area: in vitro validation and clinical implications. J Biomech. 2012; 45:1239–1245. [PubMed: 22342139]
39. Bolger AP, Sharma R, Li W, et al. Neurohormonal activation and the chronic heart failure syndrome in adults with congenital heart disease. Circulation. 2002; 106(1):92–99. [PubMed: 12093776]
40. Scammell AM, Diver MJ. Plasma renin activity in infants with congenital heart disease. Archives of disease in childhood. 1987; 62(11):1136–1138. [PubMed: 3318712]
41. Lang RE, Unger T, Ganten D, Weil J, Bidlingmaier F, Dohlemann D. Alpha atrial natriuretic peptide concentrations in plasma of children with congenital heart and pulmonary diseases. British medical journal. 1985; 291(6504):1241. [PubMed: 2933120]
42. Goodall MC, Sealy WC. Increased sympathetic nerve activity following resection of coarctation of the thoracic aorta. Circulation. 1969; 39(3):345–351. [PubMed: 5766803]
43. Canniffe C, Ou P, Walsh K, Bonnet D, Celermajer D. Hypertension after repair of aortic coarctation--a systematic review. International journal of cardiology. 2013; 167(6):2456–2461. [PubMed: 23041096]
44. Clark C. Turbulent velocity measurements in a model of aortic stenosis. J Biomech. 1976; 9:677–687. [PubMed: 1002731]
45. Cassanova RA, Giddens DP. Disorder distal to modeled stenoses in steady and pulsatile flow. J Biomech. 1978; 11:441–453. [PubMed: 730759]
46. Saad AA, Giddens DP. Velocity measurements in steady flow through axisymmetric stenoses at moderate Reynolds numbers. J Biomech. 1983; 16:505–516. [PubMed: 6619168]
47. Yoganathan KB, Chandran F, Sotiropoulos. Flow in prosthetic heart valves: state-of-the-art and future directions. Ann Biomed Eng. 2005; 33:1689–1694. [PubMed: 16389514]

48. Mittal R, Simmons SP, Najjar F. Numerical study of pulsatile flow in a constricted channel. JFM. 2003; 485:337–378.
49. Paul MC, Mamun Molla M, Roditi G. Large-Eddy simulation of pulsatile blood flow. Med Eng Phys. 2009; 31:153–159. [PubMed: 18562236]
50. Tan FP, Wood NB, Tabor G, Xu XY. Comparison of LES of steady transitional flow in an idealized stenosed axisymmetric artery model with a RANS transitional model. J Biomech Eng. 2011; 133:051001. [PubMed: 21599092]
51. Nicoud F, Ducros F. Subgrid-scale stress modeling based on the square of the velocity gradient tensor. Flow Turbulence and Combustion. 1999; 62:183–200.
52. Morris L, Delassus P, Callanan A, Walsh M, Wallis F, Grace P, McGloughlin T. 3-D numerical simulation of blood flow through models of the human aorta. J Biomech Eng. 2005; 127:767–775. [PubMed: 16248306]
53. Jin S, Oshinski J, Giddens DP. Effects of wall motion and compliance on flow patterns in the ascending aorta. J Biomech Eng. 2003; 125:347–354. [PubMed: 12929239]
54. Keshavarz-Motamed Z, Garcia J, Kadem L. Fluid dynamics of coarctation of the aorta and effect of bicuspid aortic valve. PLoS One. 2013; 8:e72394. [PubMed: 24015239]
55. Keshavarz-Motamed Z, Garcia J, Pibarot P, Larose E, Kadem L. Modeling the impact of concomitant aortic stenosis and coarctation of the aorta on left ventricular workload. J Biomech. 2011; 44:2817–2825. [PubMed: 21955730]
56. Benevento E, Dejebbari A, Keshavarz-Motamed Z, Cecere R, Kadem L. Flow distribution in aortic valve bypass: a mathematical modeling approach. PLoS One. 2015; 10(4):e0123000. [PubMed: 25881082]
57. Suga H, Sagawa K, Shoukas AA. Load independence of the instantaneous pressure-volume ratio of the canine left ventricle and effects of epinephrine and heart rate on the ratio. Circulation Research. 1973; 32:314–322. [PubMed: 4691336]
58. Senzaki H, Chen CH, Kass DA. Single-beat estimation of end-systolic pressure-volume relation in humans. A new method with the potential for noninvasive application. Circulation. 1996; 94:2497–2506. [PubMed: 8921794]
59. Saeedi, A. Thesis. 2015. Energetic and Hemodynamic Characteristics of Paravalvular Leak Following Transcatheter Aortic Valve Replacement.
60. Safar ME, Levy BL, Struijker-Boudier H. Current perspectives on arterial stiffness and pulse pressure in hypertension and cardiovascular diseases. Circulation. 2003; 107:2864–2869. [PubMed: 12796414]
61. Stergiopulos N, Segers P, Westerhof N. Use of pulse pressure method for estimating total arterial compliance in vivo. Am J Physiol. 1999; 276:424–428.

# APPENDIX

# NUMERICAL STUDY

## A. NUMERICAL MODEL

In healthy vessels, the blood flow is usually laminar and does not experience transition to turbulence. The solution was therefore obtained by simulating a laminar flow inside the domain of healthy aorta. Under physiological conditions, the blood flow may remain laminar proximal (upstream) to moderate and severe stenoses but becomes turbulent distally (44,45,46). Due to the transitional and turbulent nature of the blood flow in the human arterial system, approaches based on the Reynolds-averaged Navier Stokes (RANS) equations are the most prevalent to model. However, it was recently indicated the limitations of the predictive capability of existing RANS models for pulsatile flows (47). Direct numerical simulations (DNS) have allowed significant advances in the understanding and the modeling of turbulence, but tax computing resources and are restricted to low Reynolds

numbers. Large eddy simulation (LES) approach, which lies between DNS and RANS, is a technique well suited for the computational modelling of turbulent arterial flows, due to the finer resolution and its ability to handle transition. There have been a number of studies using LES on idealized blood vessels with a constriction (48,49,50), and very good agreement compared to experimental results was found, demonstrating the high potential of LES in modeling the physiological low-Reynolds transitional flows.

In this study, numerical simulations rely on three dimensions LES computational fluid dynamics open source (OpenFOAM). The flow was modeled using LES with the wall-adapting local eddy-viscosity (WALE) sub-grid model introduced by Nicoud and Ducros (1999) (51). LES is a technique that separates between large and small scales in the flow: the scales larger than a filter width (normally the grid spacing) are resolved while the smaller scales are handled by the WALE subgrid model. The WALE model recovers the proper $y^3$ near-wall scaling for the eddy viscosity without requiring dynamic procedure (51).

The governing equations are obtained by filtering the time-dependent continuity and Navier-Stokes equations as the followings:

$$\frac{\partial \overline{u}}{\partial x_i}=0 \quad 1$$

$$\frac{\partial}{\partial t}(\rho\overline{u}_i)+\frac{\partial}{\partial x_j}(\rho\overline{u}_i\overline{u}_j)=-\frac{\partial \overline{p}}{\partial x_i}+\frac{\partial}{\partial x_j}(\mu\frac{\partial \sigma_{ij}}{\partial x_j})-\frac{\partial \tau_{ij}}{\partial x_j} \quad 2$$

Where $\sigma_{ij}$ is the stress tensor defined by equation 3. $\tau_{ij}$ is the subgrid-scale stress defined by equation 4.

$$\sigma_{ij}=\left[\mu(\frac{\partial \overline{u}_i}{\partial x_j}+\frac{\partial \overline{u}_j}{\partial x_i})\right]-\frac{2}{3}\mu\frac{\partial \overline{u}_l}{\partial x_l}\delta_{ij} \quad 3$$

$$\tau_{ij}=\rho\overline{u_iu_j}-\rho\overline{u}_i\overline{u}_j \quad 4$$

The subgrid-scale stresses are related to the large-scale strain rate tensor $\bar{S}_{ij}$ through the eddy-viscosity hypothesis:

$$\tau_{ij}-\frac{1}{3}\delta_{ij}\tau_{kk}=2\mu_T\overline{S}_{ij} \quad 5$$

$$\overline{S}_{ij}=\frac{1}{2}\left(\frac{\partial \overline{u}_i}{\partial x_j}+\frac{\partial \overline{u}_j}{\partial x_i}\right) \quad 6$$

where $\mu_T$ is the subgrid-scale turbulent viscosity and $\bar{S}_{ij}$ is the resolves strain-rate defined by equation 6. In the WALE model, the eddy viscosity is proposed as the following:

$$\mu_T=\rho L_S^2\frac{\left(S_{ij}^d S_{ij}^d\right)^{3/2}}{\left(\overline{S}_{ij}\overline{S}_{ij}\right)^{5/2}+\left(S_{ij}^d S_{ij}^d\right)^{5/4}} \quad 7$$

Where $L_S$ and $S_{ij}^d$ in the WALE model are defined in equations 8 and 9, respectively. $L_S$ is the mixing length for subgrid scales. Where $\kappa$ is the von karman constant, d is the distance to the closest wall, $C_w$ is the WALE constant and V is the volume of the computational cell. The default value of the WALE constant, $C_w$, is 0.325 and has been found to yield satisfactory results for a wide range of flow. The $S_{ij}{}^d$ tensor can be rewritten in terms of (filtered) strain-rate ($\bar{S}_{ij}$) and vorticity ($\bar{\Omega}_{ij}$) as followings:

$$L_S=\min(\kappa d, C_w V^{1/3}) \quad 8$$

$$S_{ij}{}^d=\overline{S}_{ik}\overline{S}_{kj}+\overline{\Omega}_{ik}\overline{\Omega}_{kj}-\frac{1}{3}\delta_{ij}\left(\overline{S}_{mn}\overline{S}_{mn}-\overline{\Omega}_{mn}\overline{\Omega}_{mn}\right) \quad 9$$

where

$$\overline{\Omega}_{ij}=\frac{1}{2}\left(\frac{\partial \overline{u}_i}{\partial x_j}-\frac{\partial \overline{u}_j}{\partial x_i}\right) \quad 10$$

$$\overline{S}_{ij}=\frac{1}{2}\left(\frac{\partial \overline{u}_i}{\partial x_j}+\frac{\partial \overline{u}_j}{\partial x_i}\right) \quad 11$$

## RECONSTRUCTED GEOMETRIES IN PATIENTS WITH COA USING CT AND MRI IMAGES

We used CT and MRI images from thirty-four patients with mild COA to segment and reconstruct the 3D geometries of the complete aorta (ascending aorta, aortic branches and descending aorta) using ScanIP (version 5.3; Simpleware Ltd.), a 3D image processing and

model generation software package (Fig. 1). These 3-D reconstructions were used for investigating hemodynamic using computational fluid dynamics.

## NUMERICAL STRATEGY

A hybrid mesh of hexahedral elements was generated using open source (SALOME). Complex geometrical regions were discretized with unstructured tetrahedral and wedge elements. The Courant number was always lower than 0.9 which in turn improves accuracy of numerical simulation and reduces numerical dispersion. The non-dimensional wall distance $y^+$ ranged between 0.1–0.43 during a cardiac cycle, which ensured that the near-wall resolution was fine enough and turbulence effects were resolved accurately. The $y^+$ term is a dimensionless distance from the wall and is normally used to check where the first mesh node is located in the boundary layer. It is defined as $y^+ = \frac{yu_*}{\upsilon}$, where y is the normal distance from the wall to the first mesh node, $u_*$ the (wall) friction velocity, and $\upsilon$ the viscosity. The friction velocity is defined as $u_* = \sqrt{\frac{\tau_w}{\rho}}$ where $\tau_w$ and $\rho$ are wall shear stress and fluid density, respectively. It has been shown that the near-wall region can be divided into three layers; the innermost layer called the viscous sublayer, where viscosity plays an important role in momentum, energy and mass transfer, and the outermost layer (defect layer) where turbulence plays an important role. Between the two layers is the log layer where viscosity and turbulence are equally important. A $y^+$ value of 1 means that the first mesh node is well inside the viscous sublayer and, with reasonable growth of the mesh thickness, those consecutive mesh nodes will resolve the rest of the viscous sublayer, the log-layer and the defect layer.

Mesh independency was judged by two criteria: velocity and wall shear stress. Mesh de nition was considered as acceptable when no signi cant difference (lower than 5%) between successive meshes was noticed in wall shear stress, and also in velocity pro les. LES requires substantially finer meshes than those typically used for RANS calculations. Mesh independency test was carried and mesh independency was achieved for these two criteria for all cases. The solution marched in time with a time step 0.2 ms yielding a maximum Courant number of 0.9. In addition, LES has to be run for a sufficiently long flow-time to obtain stable statistics of the flow being modeled. Due to the transient nature of the LES model, 18 cardiac cycles were computed. Phase averages of WSS were computed using the last 10 cycles. This ensured results that were independent of sudden transient effects. Convergence was obtained when all residuals reached a value lower than $10^{-5}$. Temporal discretization was performed with a second order backward Euler scheme and the spatial discretization used second order central differencing.

## BOUNDARY CONDITIONS AND MODEL PROPERTIES

Blood was assumed to be a Newtonian and incompressible fluid with dynamic viscosity of 0.0035 Pa·s and a density of 1050 kg/m$^3$ (52). Although whole human blood tends to exhibit non-Newtonian behavior at shear rates under 100 s$^{-1}$ near the vessel walls, the shear rates in large arteries are generally observed to be greater than 100 s$^{-1}$ and hence it is reasonable to

assume a Newtonian fluid in the simulation. The arterial wall was treated as a rigid wall as Jin et al. (2003) (53) and Keshavarz-Motamed et al. (2013) (54) showed that rigid wall assumption for the aorta is realistic; and as patients with COA are usually hypertensive and characterized by reduced compliance and elevated stiffness index in both proximal and distal aorta (7,31,32,33).

A lumped-parameter model simulating the function of the left side of the heart was coupled to the inlet of the 3-D aorta model (Fig. 1; schematic diagram). Boundary conditions of the aortic branches were adjusted to match the flow distribution (Fig. 2). The outlets of the 3-D descending aorta were coupled to a three-element Windkessel models to represent the downstream vasculature networks that are absent in the 3-D computational domains. Boundary conditions were adjusted to match the flow distribution and the arterial pressure from the Doppler echocardiography and cardiac catheterization clinical data (see section B for details).

### B. LUMPED PARAMETER MODEL

The lumped-parameter model includes five sub-models: 1) LV; 2) aortic valve; 3) COA; 4) aortic regurgitation and 5) systemic circulation (Fig. 2, schematic diagram; Table 2, parameters used in the model). All input parameters were obtained from transthoracic echocardiography (TTE) measurements (Table 1). Sub-models have already been used and validated against *in vivo* MRI data in previous works (7,17,55,56). Moreover, in this study, the lumped parameter model is validated against cardiac catheterization data in thirty-four patients with mild COA (see Figures 3 to 6 for examples).

## HEART-ARTERIAL MODEL

The ventricle was filled by a normalized physiological mitral flow waveform adjusted for the required stroke volume (7,17,55). Coupling between LV pressure and volume was performed through a time varying elastance E(t), a measure of cardiac muscle stiffness.

$$E(t)=\frac{P_{LV}(t)}{V(t)-V_0} \quad (1)$$

Where $P_{LV}(t)$, $V(t)$ and $V_0$ are left ventricular time-varying pressure, time-varying volume and unloaded volume, respectively (57,58). The amplitude of E(t) can be normalized with respect to maximal elastance $E_{max}$, *i.e.*, the slope of the end-systolic pressure-volume relation, giving $E_N(t_N)=E(t)/E_{max}$. Time then can be normalized with respect to the time to reach peak elastance, $T_{Emax}$ ($t_N=t/T_{Emax}$). These normalized time-varying elastance curves $E_N(t_N)$ have similar shapes in the normal human heart under various inotropic conditions or in affected human hearts irrespective of disease etiology (57,58).

$$E_{\max}E_N(t/T_{E\max})=\frac{P_{LV}(t)}{V(t)-V_0} \quad (2)$$

This normalized curve can be described mathematically (Fourier series, polynomial description), and therefore, if $E_N(t_N)$ is given, the relation between $P_{LV}(t)$ and V(t) can be determined for the left ventricle.

## MODELING AORTIC VALVE

Aortic stenosis (AS) was modeled using the semi-analytical formulation for the net pressure gradient ($TPG_{net}$) across the stenotic valve during LV ejection. This formulation expresses the instantaneous net pressure gradient across the stenotic valve (after pressure recovery) as a function of the instantaneous flow rate and the energy loss coefficient and links the LV pressure to the ascending aorta pressure (7,17,55,56):

$$TPG_{net}\big|_{AS} = P_{LV}(t) - P_A(t) = \frac{2\pi\rho}{\sqrt{E_L Co\big|_{As}}}\frac{\partial Q(t)}{\partial t} + \frac{\rho}{2E_L Co\big|_{AS}^2}Q^2(t) \quad (3)$$

and

$$E_L Co\big|_{AS} = \frac{(EOA\big|_{COA})A}{A - EOA\big|_{AS}} \quad (4)$$

where $E_L Co|_{AS}$, $EOA|_{AS}$, $A$, $\rho$ and $Q$ are the valvular energy loss coefficient, the effective orifice area, ascending aorta cross sectional area, the fluid density and the transvalvular flow rate, respectively. $E_L CO|_{AS}$, representing the 'recovered EOA', denotes valve effective orifice area adjusted for the area of the aorta at the level of sinotubular junction. Therefore, variable aortic valve resistance ($R_{av}$) and constant aortic valve inductance ($L_{av}$) (Figures 1 and 2) in the lumped parameter model are $\frac{\rho}{2E_L CO\big|_{AS}^2}$ and $\frac{2\pi\rho}{\sqrt{E_L CO\big|_{AS}}}$, respectively

## MODELING AORTIC VALVE REGURGITATION

Aortic regurgitation (AR) was modeled (equations 5 and 6) using the same analytical formulation as aortic stenosis. AR pressure gradient is the difference between aortic pressure and LV pressure during diastole (59).

$$TPG_{net}\big|_{AR} = \frac{2\pi\rho}{\sqrt{E_L Co\big|_{AR}}}\frac{\partial Q(t)}{\partial t} + \frac{\rho}{2E_L Co\big|_{AR}^2}Q^2(t) \quad (5)$$

and

$$E_L Co|_{AR} = \frac{(REOA)A_{LVOT}}{A_{LVOT} - REOA} \quad (6)$$

where $E_L Co|_{AR}$, $REOA$ and $A_{LVOT}$ are regurgitation energy loss coefficient, regurgitant effective orifice area and LVOT area, respectively. The $REOA$ is calculated by dividing the regurgitant volume by the time-velocity integral of regurgitant flow using continuous wave Doppler.

## MODELING COARCTATION OF THE AORTA

The characteristics of the arterial system are of primary importance when modeling COA since only a portion of total flow rate will cross the COA. To take this into account in the model two parallel branches were considered. The first branch simulates the flow towards the upper body, or the flow bypassing the COA (including aortic arch arteries and potential collaterals). A second branch simulates the flow crossing COA and directed towards descending aorta. This branch includes a resistance for the proximal descending aorta, and a time-varying resistance and an inductance which together represent the trans-coarctation net pressure gradient induced by the COA:

$$TPG_{net}|_{COA} = \frac{2\pi\rho}{\sqrt{E_L Co|_{COA}}} \frac{\partial Q(t)}{\partial t} + \frac{\rho}{2E_L Co|^2_{COA}} Q^2(t) \quad (3)$$

And

$$E_L Co|_{COA} = \frac{(EOA|_{COA})A}{A - EOA|_{COA}} \quad (4)$$

where $E_L Co|_{COA}$, $EOA|_{COA}$, $A$, $\rho$ and $Q$ are the energy loss coefficient of the COA, the effective orifice area of the COA, aortic cross sectional area downstream of the COA, the fluid density and the trans- coarctation flow rate, respectively. The energy loss coefficient is then expressed in terms of the aortic cross section just downstream of the COA and the effective orifice area of the COA (55).

## DETERMINING ARTERIAL COMPLIANCE AND PERIPHERAL RESISTANCE

The total systemic resistance was computed as the quotient of the average brachial pressure and the cardiac output (assuming a negligible peripheral venous pressure (mean ~ 5 mmHg) compared to aortic pressure (mean ~ 100 mmHg). This total systemic resistance represents the electrical equivalent resistance for all resistances in the current model. Because what the left ventricle faces is the total systemic resistance and not the individual resistances, for the sake of simplicity we considered the aortic resistance, $R_{ao}$, and systemic vein resistance,

$R_{SV}$, as constants and adjusted the systemic artery resistance, $R_{SA}$, according to the obtained total systemic resistance.

Physiologically, arterial hypertension is determined by two factors (60): the degree of reduction in the caliber of small arteries or arterioles with an ensuing increase in systemic vascular resistance and mean blood pressure, and the extent of reduction in the arterial compliance with a resulting increase in pulse pressure (systolic minus diastolic blood pressure). For each degree of hypertension we fit the predicted pulse pressure to the actual pulse pressure (known by arm cuff sphygmomanometer) obtained from clinical study by adjusting compliances (proximal COA ($C_{ao}$) and systemic ($C_{SAC}$)). Therefore, compliance adjustment was done by a simple trial and error for each degree of hypertension (7,17,61).

## COMPUTATIONAL ALGORITHM

A lumped parameter model developed and described in detail elsewhere (7,17,55) was analyzed numerically by creating and solving a system of ordinary differential equations in Matlab Simscape (MathWorks, Inc.), enhanced by adding additional codes to meet demands of cardiac model in circuit. A Fourier series representation of an experimental normalized elastance curve for human adults (58) was used to generate a signal to be fed into the main program. Simulations start at the onset of isovolumic contraction. Left ventricle volume, V(t), is calculated using left ventricle pressure, $P_{LV}$, and time varying elastance values (equation 1). $P_{LV}$ used in the beginning of calculation is the initial value assumed across the variable capacitor and is automatically adjusted later by system of equations as solution advances. Left ventricle flow rate subsequently was calculated as time derivative of left ventricle volume. Matlab's ode23t trapezoidal rule variable-step solver was used to solve system of differential equations with initial time step of 0.1 milliseconds. The convergence residual criterion was set to $10^{-5}$ and initial voltages and currents of capacitors and inductors set to zero.

## PERSPECTIVES

### WHAT'S KNOWN?

The optimal method and timing of transcatheter intervention for COA remains unclear, especially when the severity of COA is mild.

### WHAT'S NEW?

In all studied thirty-four patients with mild COA, transcatheter intervention can effectively reduce the trans-coarctation pressure gradient however this results in only a modest local improvement in aortic hemodynamics, and does not translate to a concomitant improvement in LV hemodynamics or reduction in myocardial strain. Our findings suggest that how the definition of "mild coarctation", based on peak-to-peak trans-coarctation pressure gradient of 20 mmHg, is an oversimplification and suggest more accurate assessments of this class of patients for deciding about performing a transcatheter intervention.

### WHAT'S NEXT?

Future studies must not only consider the upstream but also downstream effects of coartation repair when determining indication and assessing benefit of intervention.

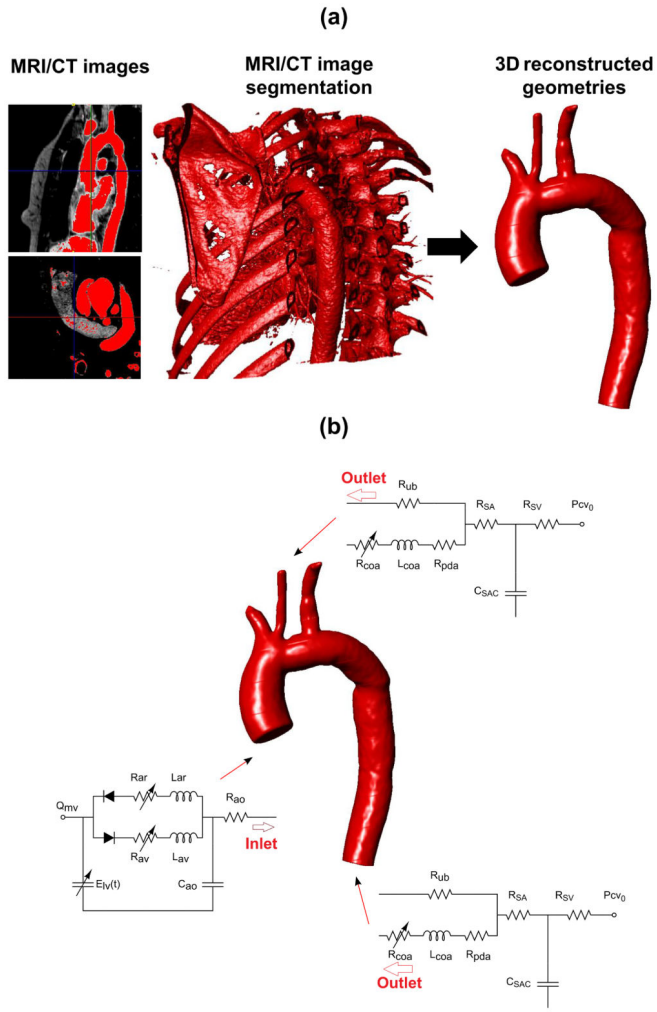


**Figure 1.**

(a) Reconstructed 3D geometries in patients with COA using CT and MRI images. Geometries were used for investigating hemodynamic using computational fluid dynamics and lumped parameter modeling; (b) Schematic diagram of simulation domain. A lumped-parameter model simulating the function of the left side of the heart is coupled to the inlet of the aorta model. Boundary conditions of the aortic branches are adjusted to match the flow distribution. The outlets of the 3-D descending aorta is coupled to a three-element Windkessel models to represent the downstream vasculature networks that are absent in the 3-D computational domains.

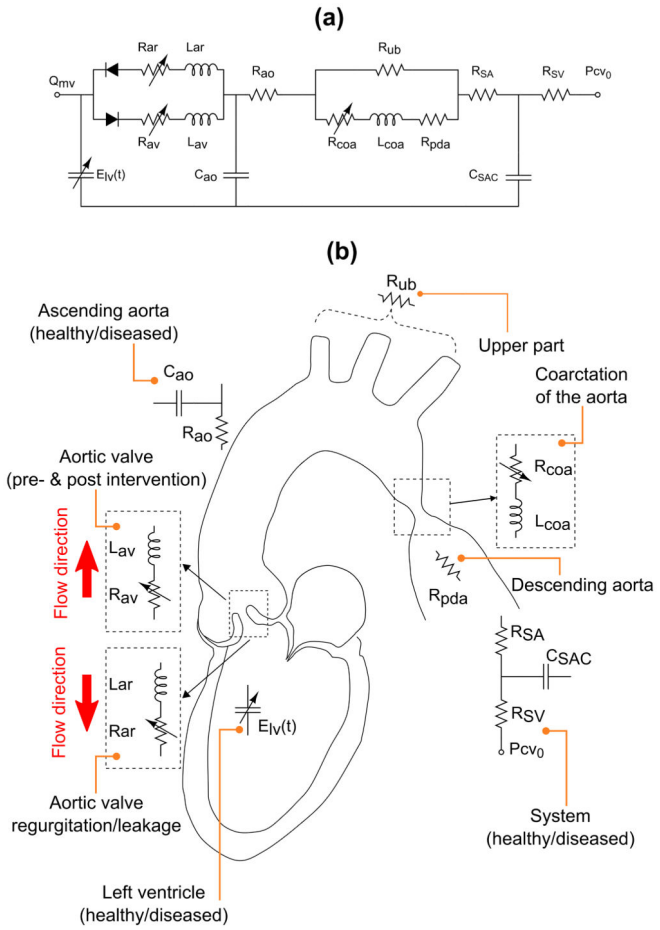


**Figure 2.**

Schematic diagram of the lumped parameter model. (a) electrical representation, (b) anatomical representation. Abbreviations are similar as in Table 1.

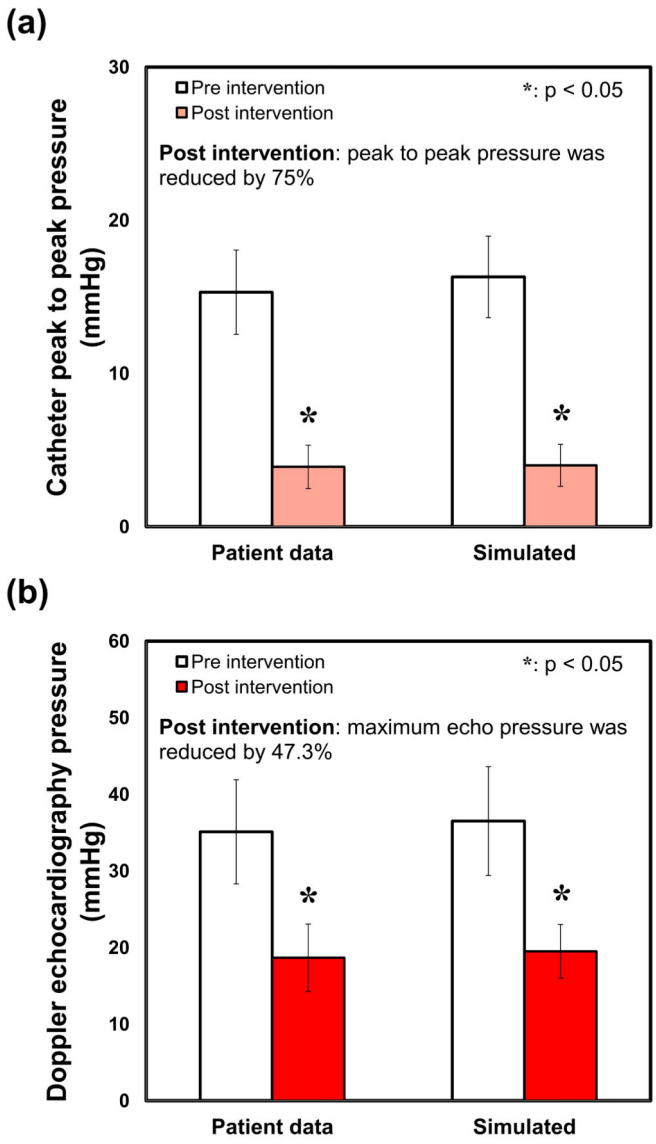


**Figure 3.**

(a) Differences in the catheter peak to peak pressure gradient between pre and post intervention conditions (*: $p<0.05$ compared with peak to peak pressure gradient of pre intervention; N=34); (b) Differences in the Doppler echocardiography pressure gradient between pre and post intervention conditions (*: $p<0.05$ compared with Doppler pressure gradient of pre intervention; N=34).

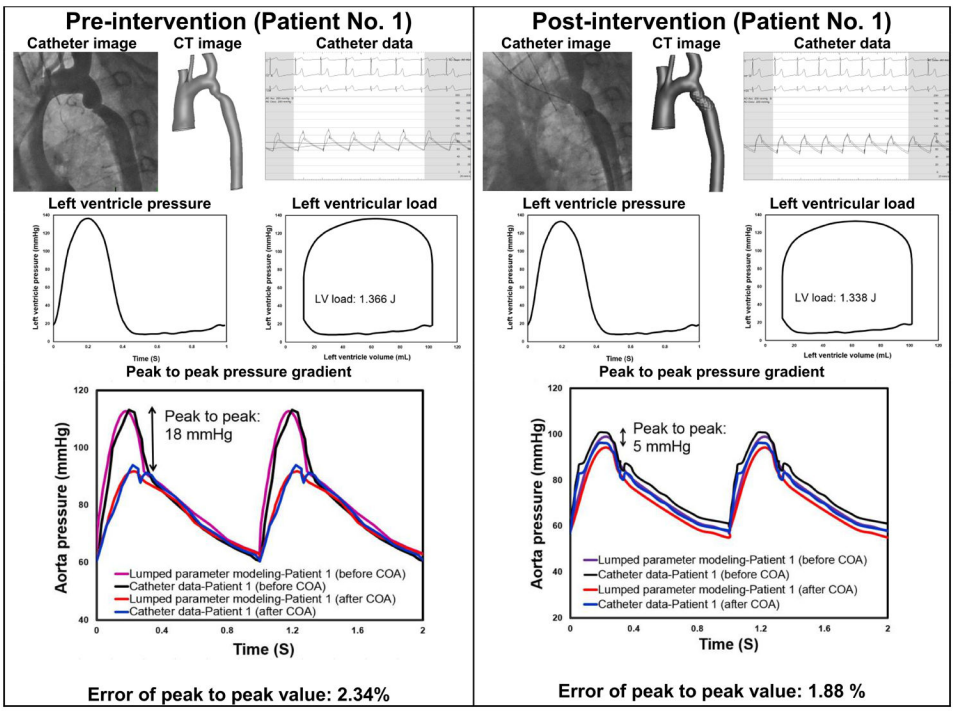


**Figure 4.**

Catheter data and results of lumped parameter modeling in patient No. 1. Pre intervention: there was an 18 mmHg peak-to-peak pressure gradient across the coarctation site. Doppler flow patterns in the abdominal aorta show mild delay in systolic upstroke, mid-systolic turbulence and low velocity anterograde flow throughout diastole. Post intervention: the stent was deployed with mild residual stenosis due to malapposition of the stent proximal to the coarctation. The gradient was abolished post stenting and peak-to-peak pressure gradient across the stent decreased to 5 mmHg. Angiography post dilatation did not reveal a dissection or extravasation of contrast. The patient tolerated the procedure well without complication.

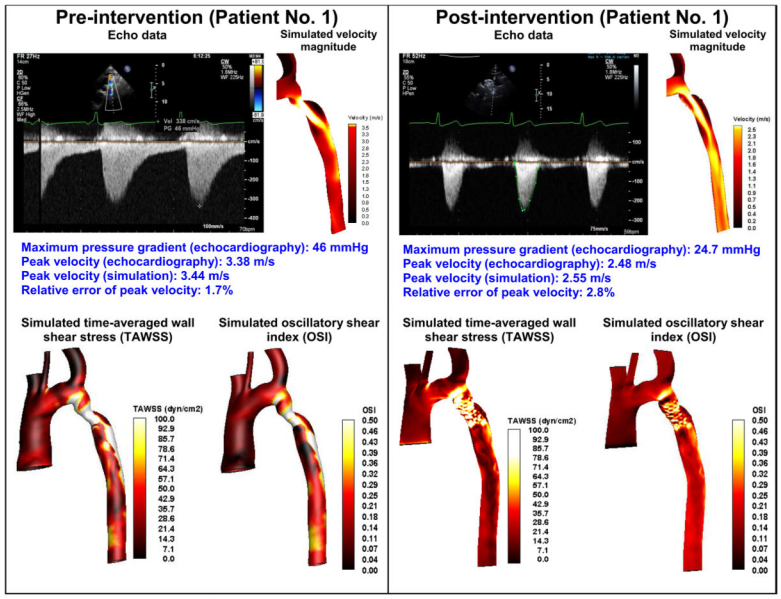


**Figure 5.**

Echocardiography data and results of lumped parameter and computational fluid dynamics modeling in patient No. 1.

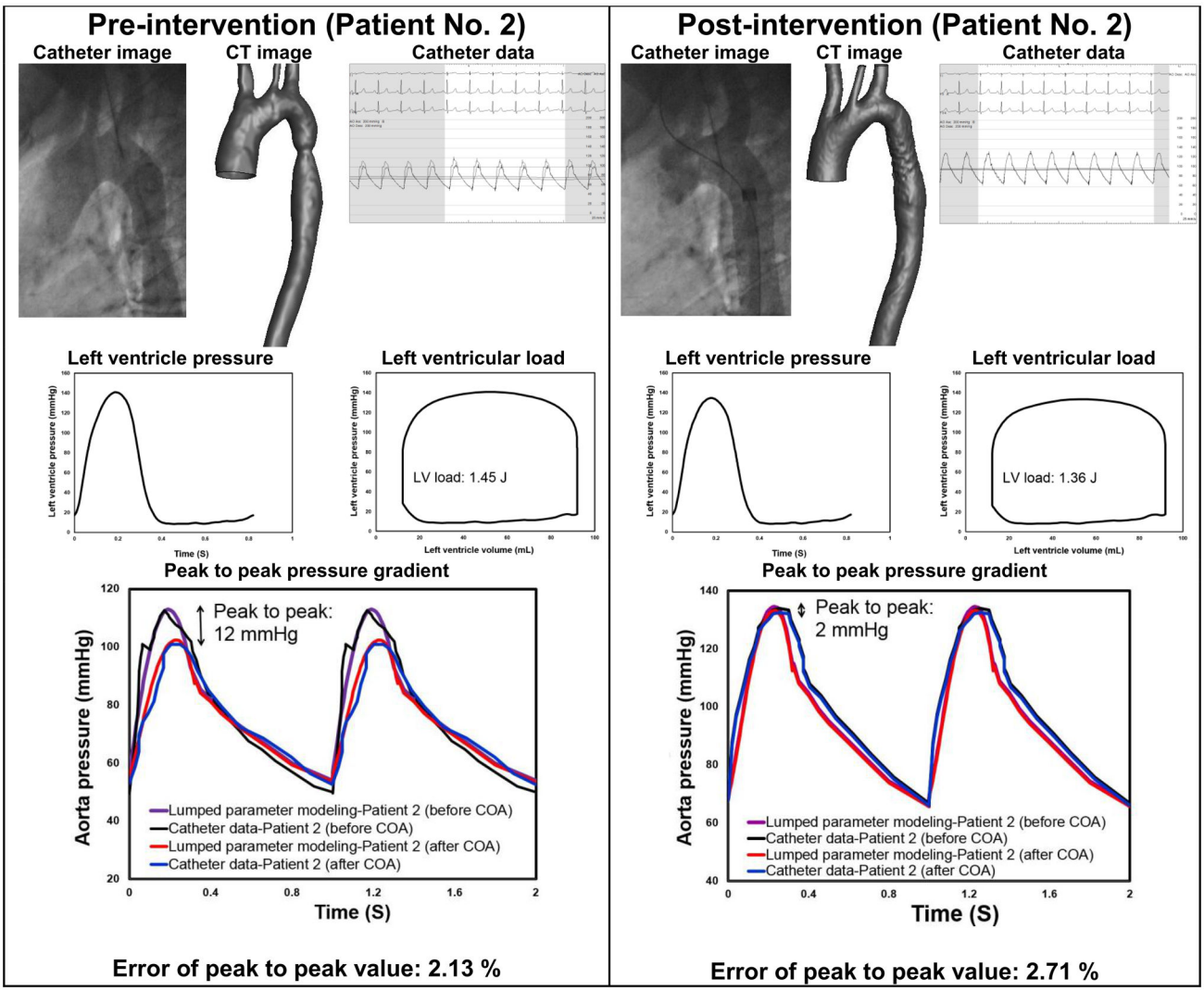


**Figure 6.**

Catheter data and results of lumped parameter modeling in patient No. 2. Pre intervention: there was a 12 mmHg peak-to-peak pressure gradient across the coarctation site. There was an evidence of mild aortic valve stenosis. Post intervention: the stent was successfully deployed without residual stenosis. Angiography and pressure measurement confirmed stent expansion with no extravasation, contrast staining or hemodynamic instability. Final pressure measurement using a catheter revealed no residual gradient across the coarctation site and peak-to-peak pressure gradient across the stent was 2 mmHg. There was no evidence of aneurysm or dissection. The patient tolerated the procedure well without complication.

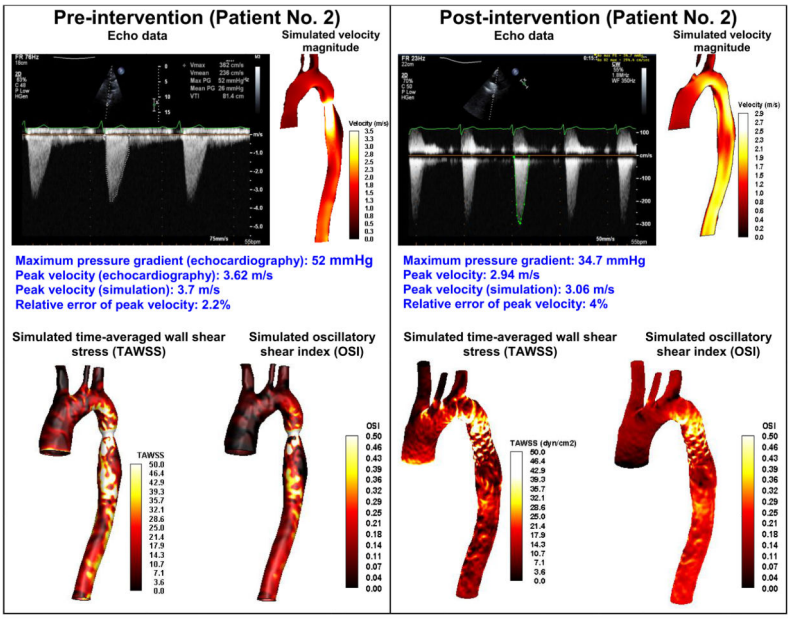


**Figure 7.**

Echocardiography data and results of lumped parameter and computational fluid dynamics modeling in patient No. 2.

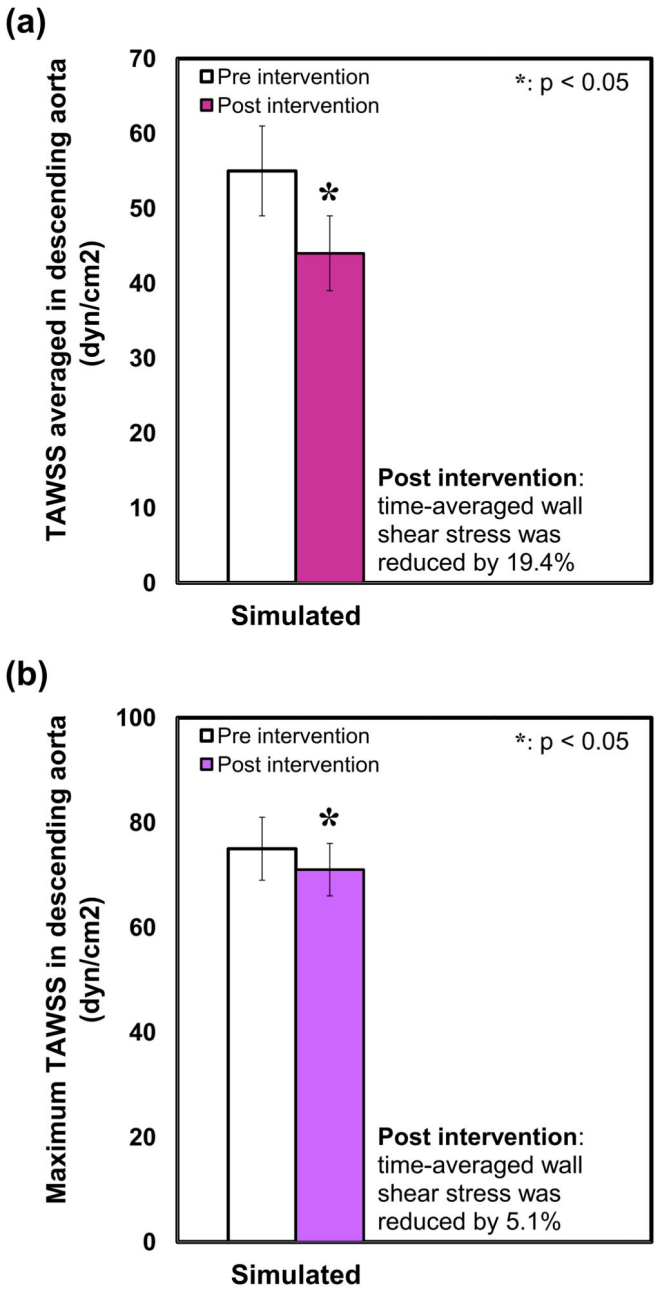


**Figure 8.**

Differences in the time-averaged wall shear stress between pre and post intervention conditions (*: p<0.05 compared with TAWSS of pre intervention; N=34). The total shear stress exerted on the wall throughout the cardiac cycle was evaluated using the time-averaged wall shear stress (TAWSS) which is obtained as $TAWSS=\frac{1}{T}\int_0^T |\tau|\, dt$. Here, T and $\boldsymbol{\tau}$ are the cardiac cycle period and instantaneous wall shear stress, respectively.

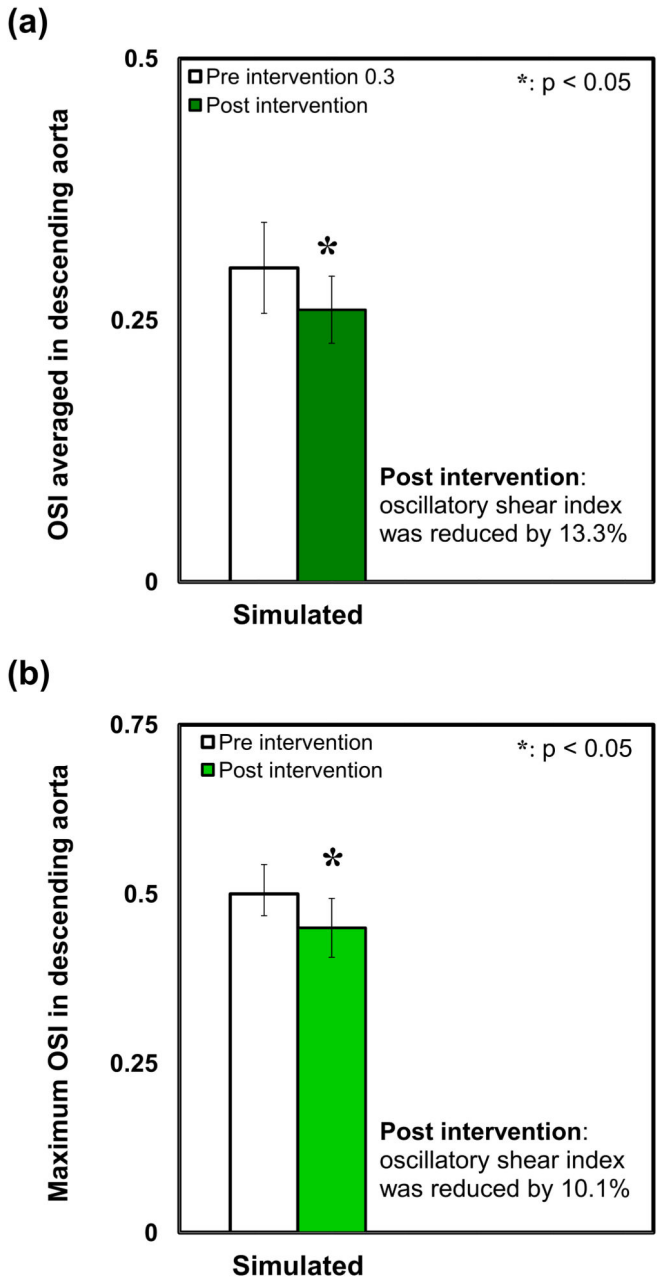


**Figure 9.**

Differences in the oscillatory shear index between pre and post intervention conditions (*: p<0.05 compared with TAWSS of pre intervention; N=34). To evaluate temporal oscillations in wall shear stress, the oscillatory shear index (OSI) was used as $$OSI = 1/2 \left( 1 - \frac{\int_0^T \tau dt}{\int_0^T |\tau| \, dt} \right).$$ Here, T and $\boldsymbol{\tau}$ are the cardiac cycle period and instantaneous wall shear stress, respectively.

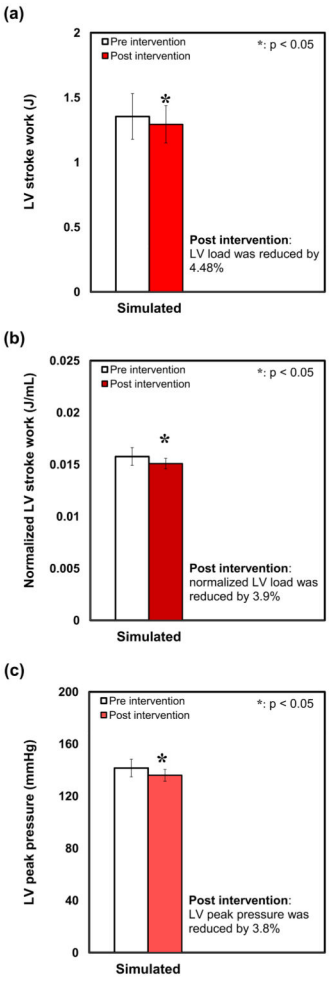


**Figure 10.**

(a) Differences in the LV stroke work between pre and post intervention conditions (*: $p<0.05$ compared with LV stroke work of pre intervention; N=34); (b) Differences in the normalized LV stroke work between pre and post intervention conditions (*: $p<0.05$ compared with normalized LV stroke work of pre intervention; N=34). Normalized stroke work represents the energy required to eject 1 mL of blood through the valvulo-arterial system; (c) Differences in the LV peak pressure between pre and post intervention conditions (*: $p<0.05$ compared with LV peak pressure of pre intervention; N=34).

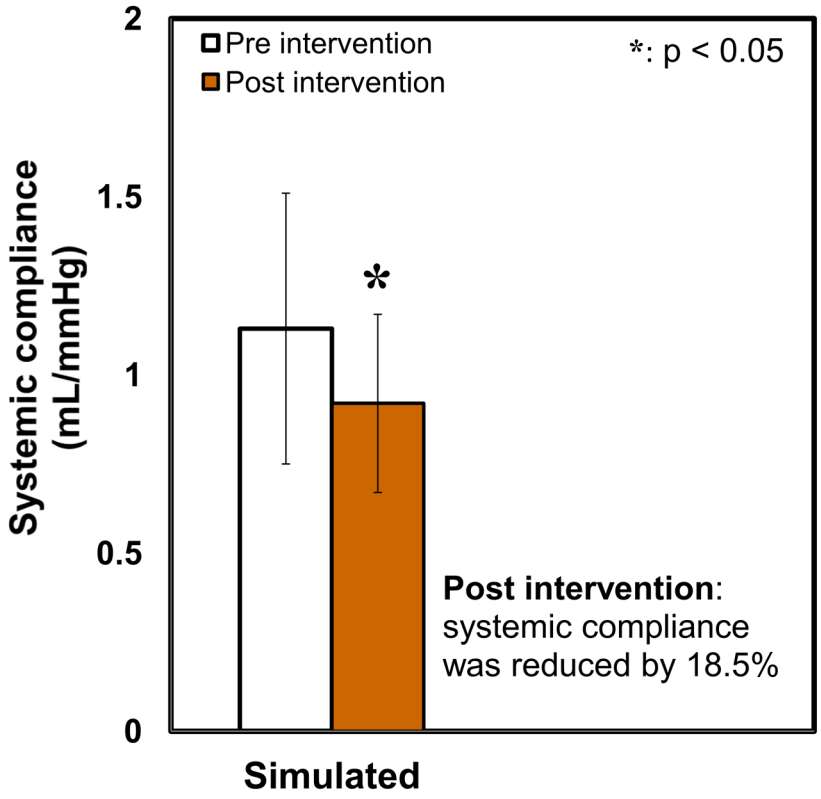


**Figure 11.**

Differences in the systemic arterial compliance between pre and post intervention conditions (*: $p<0.05$ compared with systemic arterial compliance of pre intervention; N=34).

## Table 1

Baseline patient characteristics.

| | COA Patients (n=34, mean ± SD) |
|---|---|
| **Patient description** | |
| Mean age (years) | 41 ± 10.5 |
| Gender (n) | (Female:18; male: 16) |
| Mean weight (kg) | 77 ± 17.4 |
| Body surface area ($m^2$) | 1.9 ± 0.25 |
| Stroke volume (SV) (mL) | 77.4 ± 17.9 |
| Heart rate (beats/min) | Pre intervention: 65 ± 11; Post intervention: 64 ± 13 |
| **Arterial hemodynamics** | |
| Systemic arterial compliance (SAC) ($mL.mmHg^{-1}$) | Pre intervention: 1.13 ± 0.38; Post intervention: 0.92 ± 0.25 |
| Systolic arterial pressure (mmHg) | Pre intervention: 139 ± 22.5; Post intervention: 129 ± 16.8 |
| Diastolic arterial pressure (mmHg) | Pre intervention: 79 ± 11.7; Post intervention: 73 ± 10.3 |
| **Coarctation description** | |
| Proximal to COA diameter (mm) | Pre intervention: 18 ± 5.9; Post intervention: 19.5 ± 4.3 |
| COA diameter (mm) | Pre intervention: 13.2 ± 4.5; Post intervention: 16.5 ± 1.9 |
| Distal to COA diameter (mm) | Pre intervention: 25.5 ± 2.1; Post intervention: 24.5 ± 3.1 |
| Diameter ratio (COA/Aorta) | Pre intervention: 0.72 ± 0.25; Post intervention: 0.94 ± 0.27 |
| Catheter peak to peak pressure gradient (mmHg) | Pre intervention: 15.3 ± 2.9; Post intervention: 3.9 ± 1.4 |
| Catheter mean pressure gradient (mmHg) | Pre intervention: 7.3 ± 3.3; Post intervention: 1.9 ± 0.4 |
| Doppler maximum pressure gradient (mmHg) | Pre intervention: 35.1 ± 6.8; Post intervention: 18.6 ± 4.4 |
| Doppler mean pressure gradient (mmHg) | Pre intervention: 17 ± 5.4; Post intervention: 9.7 ± 3.5 |
| **Cardiac catheterization** | |
| Stent size: diameter (mm) & length (mm) | (12.8 ± 3.3) & (32.8 ± 5.11) |
| Balloon size: diameter (mm) & length (mm) | (17.4 ± 6.8) & (34.6 ± 8.4) |
| **Valve hemodynamics** | |
| Effective orifice area ($cm^2$) | 2.6 ± 0.48 |
| Doppler maximum pressure gradient (mmHg) | 17.9 ± 9.6 |
| Doppler mean pressure gradient (mmHg) | 10.6 ± 4.3 |
| **Associated cardiovascular lesions** | |
| Bicuspid aortic valve (BAV) | 10 |
| Tricuspid aortic valve stenosis (AS) | 3 |
| Unicuspid valve | 1 |
| Ventricular septal defect | 1 |
| Mitral valve regurgitation | 4 |
| Descending aorta aneurysms | 3 |
| Collaterals | 2 |

**Table 2**

Summarized cardiovascular parameters used in the lumped parameter modeling to simulate all cases.

| Description | Abbreviation | Value |
|---|---|---|
| **COA and valve parameters** | | |
| Effective orifice area | EOA | From echocardiography data |
| Energy loss coefficient | $E_L$Co | $\frac{(EOA)A}{A-EOA}$ From echocardiography data |
| Variable resistance | $R_{coa}$ & $R_{av}$ & $R_{ar}$ | $\frac{\rho}{2E_L Co^2}Q$ |
| Inductance | $L_{coa}$ & $L_{av}$ & $L_{ar}$ | $\frac{2\pi\rho}{\sqrt{E_L Co}}$ |
| **Systematic circulation parameters** | | |
| Aortic resistance | $R_{ao}$ | 0.05 mmHg.s.mL$^{-1}$ |
| Aortic compliance | $C_{ao}$ | Initial value: 0.5 mL/mmHg<br>Adjust for each degree of hypertension (Proximal COA compliance) |
| Systemic vein resistance | $R_{SV}$ | 0.05 mmHg.s.mL$^{-1}$ |
| Systemic arteries and veins compliance | $C_{SAC}$ | Initial value: 2 mL/mmHg<br>Adjust for each degree of hypertension (Systemic compliance) |
| systemic arteries resistance (including arteries, arterioles and capillaries) | $R_{SA}$ | 0.8 mmHg.s.mL$^{-1}$<br>Adjust according to the calculated total systemic resistance |
| Upper body resistance | $R_{ub}$ | Adjusted to have 15% of total flow rate in healthy case (7,50) |
| Proximal descending aorta resistance | $R_{pda}$ | 0.05 mmHg·s·mL$^{-1}$ |
| **Output condition** | | |
| Central venous pressure | $P_{CV0}$ | 4 mmHg |
| **Input condition** | | |
| Mitral valve mean flow rate | $Q_{mv}$ | From echocardiography data |
| **Other** | | |
| Constant blood density | | 1050 kg/m$^3$ |
| Heart rate | HR | From echocardiography data |
| Duration of cardiac cycle | T | From echocardiography data |